R-matrix calculation of bound and resonant states of BeH

2015 J. Phys. B: At. Mol. Opt. Phys. 48 235202

(http://iopscience.iop.org/0953-4075/48/23/235202)

IOP Publishing Journal of Physics B: Atomic, Molecular and Optical Physics
J. Phys. B: At. Mol. Opt. Phys. **48** (2015) 235202 (6pp) doi:10.1088/0953-4075/48/23/235202

R-matrix calculation of bound and resonant states of BeH

K Chakrabarti[1] **and Jonathan Tennyson**[2]

[1] Department of Mathematics, Scottish Church College, 1 & 3 Urquhart Sq., Kolkata 700006, India
[2] Department of Physics and Astronomy, University College London, Gower St., London WC1E 6BT, UK

E-mail: j.tennyson@ucl.ac.uk

Received 1 August 2015, revised 31 August 2015
Accepted for publication 4 September 2015
Published 6 October 2015

Abstract

Bound and resonant states of BeH are studied using the diatomic UK molecular R-matrix codes together with a Slater basis set for the BeH^+ target states. Bound and resonant states of BeH are determined from an e-BeH^+ collisional calculation. The calculations are repeated for 40 internuclear distances in the range 1.5–6.0 a_0 to yield bound state and resonance curves for BeH. Additionally, we also obtain the resonance widths in the range of the inter-nuclear distances considered. The data obtained may be useful for modeling various e-BeH^+ collision-induced processes, particularly dissociative recombination and dissociative excitation.

Keywords: resonance curves, Rydberg states, dissociative recombination

(Some figures may appear in colour only in the online journal)

1. Introduction

Beryllium, along with tungsten, is used as the wall material for ITER (originally the International Thermonuclear Experimental Reactor) (Merola *et al* 2014), the international fusion reactor currently under construction. The presence of H^+ (D^+, T^+) ions in plasma is likely to lead to the formation of significant quantities of BeH^+ (BeD^+, BeT^+) in the cooler divertor region, even though the exact formation process of BeH^+ in this region is not yet well understood. The main processes leading to the destruction of BeH^+ ions in plasma are likely to be dissociative recombination (DR) with electrons and electron impact dissociative excitation (DE). Collision of free electrons with BeH^+ leads to the release and subsequent redeposition of beryllium on the divertor. The motivation for the present paper is to provide *ab initio* data that can be the starting point for the calculation of the DR and DE rate coefficients needed to model Beryllium release.

Several calculations for the bound states of BeH have been undertaken. Early calculations were performed by Cooper (1984), and Henriet and Verhaegen (1984, 1986). Petsalakis *et al* (1992, 1999) calculated adiabatic $^2\Sigma^+$, $^2\Pi$ and $^2\Delta$ states of BeH using the multireference doubles-configuration interaction (MRD-CI) approach. Additionally, they also gave a procedure to construct quasidiabatic $^2\Sigma^+$ states. Detailed calculations for the $^2\Pi$ states of BeH were performed by Machado *et al* (1998) using a multireference configuration interaction approach. Full configuration interaction (FCI) calculation of low-lying valence and Rydberg states of BeH were made by Pitarch-Ruiz *et al* (2007, 2008). More recently, Roos *et al* (2009) used the multireference conguration interaction (MRCI) method to get the adiabatic and diabatic BeH states of $^2\Sigma^+$, $^2\Pi$ and $^2\Delta$ symmetry. They also produced resonance energy positions and widths using the complex Kohn variational method and subsequently used the data for a dissociative recombination calculation of BeH^+.

In a previous paper (Chakrabarti and Tennyson 2012), which will be referred to as I below, we presented cross-sections for electronic and rotational excitation for electron collision with the BeH^+ at its equilibrium bond length, $R_e = 2.5369\ a_0$. The calculation additionally yielded the bound states of BeH, resonance positions, and widths restricted to this single geometry. Here we present a more complete calculation over 40 internuclear distances in the range 1.5–6.0 a_0 to get the BeH bound states, resonance positions, and widths as a function of internuclear distance.

2. Calculations

2.1. Method

The method employed here was detailed in our earlier work I but we outline it briefly. We use the R-matrix (Tennyson 2010, Burke 2011) method that starts by dividing the configuration space into an inner region defined by a sphere centered at the molecular center-of-mass and that encloses the N-electron target BeH^+ ion. In this inner region, the wave function of the $(N + 1)$-electron system (BeH^+ + electron) is given by

$$\Psi_k = \mathcal{A}\sum_{i,j} a_{i,j,k}\Phi_i(1, \ldots, N)F_{i,j}(N + 1) + \sum_i b_{i,k}\chi_i(1, \ldots, N + 1), \quad (1)$$

where $\mathcal{A}$ is the anti-symmetrization operator, $F_{i,j}$ are continuum orbitals, and χ_i are two-center L^2 functions constructed from N-electron target orbitals. The L^2 functions allow for polarization of the N-electron target wavefunction in the presence of the projectile electron.

We use the diatomic version of the UK molecular R-matrix codes (Morgan *et al* 1998), which uses Slater type orbitals (STOs) to represent the target, and numerical orbitals in a partial wave expansion to represent the continuum (Tennyson and Morgan 1999). A Buttle correction (Buttle 1967) is used to allow for the arbitrary fixed boundary conditions imposed on the continuum basis orbitals.

2.2. BeH^+ target

Extensive tests on STOs and different target models were performed and discussed in our earlier work, I. The STO basis sets of (Bagus *et al* 1973) were chosen as they give the best agreement with existing calculations for the target excitation energies. The STOs were used to build a basis of 31 molecular orbitals comprising 17σ, 9π, 4δ, and 1ϕ orbitals. An initial SCF calculation was then performed for the lowest X $^2\Sigma^+$ state of BeH^+ using these molecular orbitals. Finally, 17σ, 9π, and 4δ SCF molecular orbitals were used in a CI calculation. A complete active space (CAS) target model $(1\sigma$-$6\sigma, 1\pi, 2\pi)^4$ was finally selected after several tests as it gave the best vertical excitation energies both for the target and the BeH bound states (see tables 1 and 3 in I).

2.3. BeH model

Calculations were based on the use of the same BeH^+ SCF orbitals and CAS. These were supplemented by continuum orbitals F_{ij} obtained as a truncated partial wave expansion around the center of mass. Partial waves with $l \leqslant 6$ and $m \leqslant 2$ were retained in the calculation. The radial parts of the continuum functions were generated as numerical solutions of an isotropic Coulomb potential and solutions with an energy below 10 Ryd were retained. An R-matrix radius 11.0 a_0 was used for internuclear separation $R \leqslant 3.0\,a_0$. This produced 175 (70σ, 58π, 47δ) continuum functions. For $R > 3.0\,a_0$ it was found necessary to increase the R-matrix radius to 15.0 a_0 to allow for the more extended nature of the target wave function, resulting in 247 (98σ, 82π, 67δ) continuum functions. The continuum functions were Schmidt orthogonalized to the target SCF orbitals. Scattering calculations were then performed using $(1\sigma$-$6\sigma, 1\pi, 2\pi)^4$ CAS target wave function for the BeH states with $^2\Sigma^+$, $^2\Pi$, and $^2\Delta$ total symmetries to yield the bound states and resonance parameters. Extensive tests were performed on the number of target states to be used in the close coupling expansion equation (1) in I. Finally, a 9-state model (3 $^1\Sigma^+$, 3 $^3\Sigma^+$, 2 $^1\Pi$ and 1 $^3\Pi$) for the BeH $^2\Sigma^+$ and $^2\Pi$ states and an 8-state model (3 $^1\Sigma$ + , 3 $^3\Sigma^+$, 1 $^1\Pi$, and 1 $^3\Pi$) for the BeH $^2\Delta$ state were used as these gave the best vertical excitation for the respective states at $R = R_e = 2.5369\ a_0$, (see I).

2.4. Bound states

The inner region solutions obtained were used to construct an R-matrix on the boundary. In the outer region, the potential was given by the diagonal and off-diagonal dipole and quadrupole moments of the BeH^+ target states in addition to the Coulomb potential. For the present work the R-matrices were propagated to 50.01 a_0 and an improved Runge-Kutta–Nystrom procedure implemented by Zhang *et al* (2011) was used. Bound states were then found using the searching algorithm of Sarpal *et al* (1991) with the improved nonlinear, quantum defect-based grid of Rabadán and Tennyson (1996).

In I we presented the number and symmetries of the states the used in the close coupling equation (1), and a detailed comparison of the vertical excitation energies from the $X\ ^2\Sigma^+$ ground state of BeH with other works, at $R_e = 2.5369\ a_0$. Hence, we do not present them here again.

2.5. Resonances

For the resonance calculation, the R-matrix were propagated (Morgan 1984) to 70 a_0, as tests showed that this produced stable results. It was then matched with asymptotic Coulomb functions (Barnett 1982) obtained using the Gailitis expansion procedure of Noble and Nesbet (1984). Resonances were detected and fitted to a Breit–Wigner profile to obtain their energy (E) and width (Γ) using the RESON program (Tennyson and Noble 1984) with an energy grid 0.5×10^{-3} Ryd. The magnitudes of the complex quantum defects $\mu = \alpha + i\,\beta$ were obtained using the relations (Tennyson 1988)

$$E_r = E_t - \frac{1}{\nu^2}, \quad \Gamma = \frac{2\beta}{\nu^3}, \quad (2)$$

where the effective quantum number ν equals $n - \alpha$ and E_t is the energy of the threshold to which the Rydberg series converges.

3. Results

3.1. Rydberg states as a function of bond length

To obtain the potential energy curves (PECs) for the Rydberg states of BeH we performed the bound state calculations outlined above for 40 inter-nuclear distances in the range $1.5 \leqslant R \leqslant 6.0\ a_0$. Figure 1 shows the PECs of BeH for $^2\Sigma^+$, $^2\Pi$,

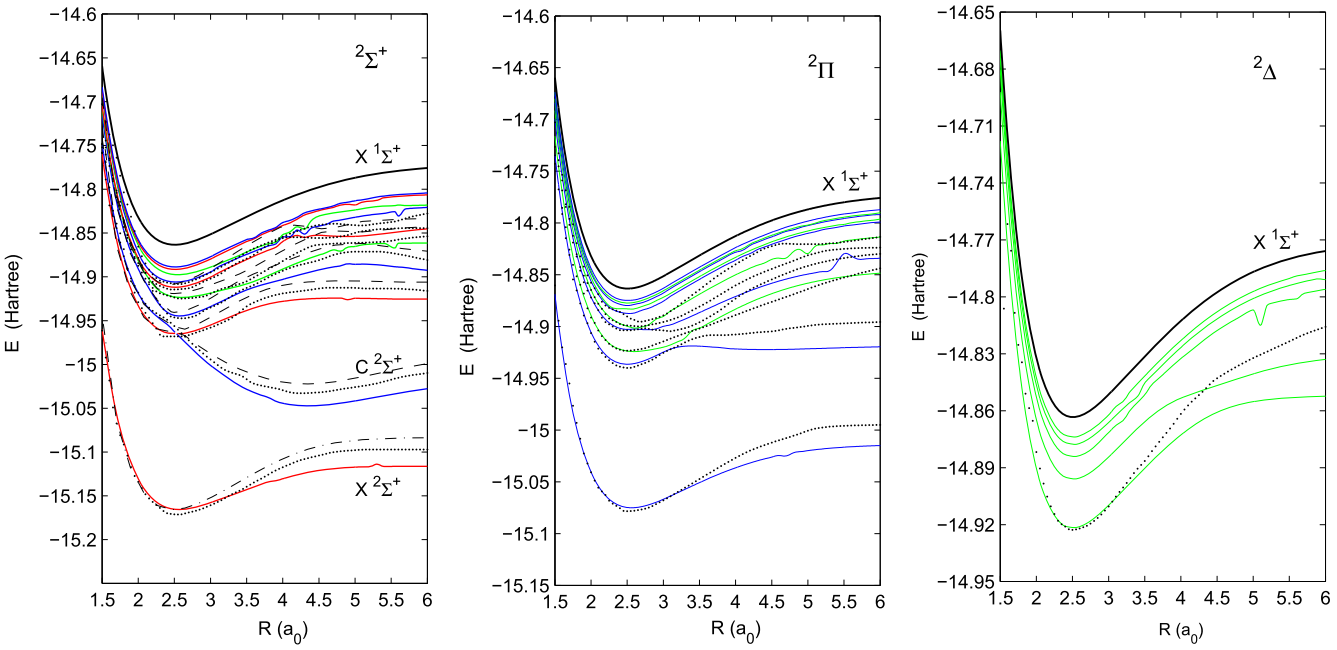

Figure 1. BeH bound state curves of $^2\Sigma^+$, $^2\Pi$, and $^2\Delta$ symmetry. Continuous curves: present calculation. Black dotted curves: (Petsalakis *et al* 1999) translated upwards by 0.04 eV. Black dash-dotted curves in the $^2\Sigma^+$ figure: Pitarch-Ruiz *et al* (2007, 2008) translated upward by 0.04 eV. The topmost thick black curve in each figure is the $X\ ^1\Sigma^+$ ground state of BeH^+.

and $^2\Delta$ symmetries. We have also included the available curves of Petsalakis *et al* (1992, 1999) (black dotted curves) for comparison. Our curves agree reasonably well with those of Petsalakis *et al* translated upward by 0.04 eV, and except the lowest $^2\Delta$ state, all other curves deviate by less than 0.7 eV from those of Petsalakis *et al* at the large R end. The differences in the $^2\Delta$ symmetry are probably caused by our use of a more complete set of δ basis functions.

Beyond $R = 4.0\,a_0$ our curves show many perturbations due to the presence of intruder states. These states, sometimes called interloper states (Ballance *et al* 1998), are usually caused by crossings with low-n members of Rydberg series associated excited states of the ion. Such crossings are more common at large R since the vertical excitation energies often decrease significantly at long bondlength. The effects of intruder states can be seen as both avoided crossings in the potential energy curves (Little and Tennyson 2013) and perturbations in the R-dependent quantum defects (Rabadán and Tennyson 1996).

We also compared our bound state curves with the full configuration interaction (FCI) curves of Pitarch-Ruiz *et al* (2007, 2008). However, we found that even though the FCI is supposed to be an exact calculation, limited only by the choice of basis sets and proper convergence, beyond $R = 2.6\,a_0$ the FCI curves deviated from ours much more than those of Petsalakis *et al*. A comparison of our curves with those of Pitarch-Ruiz *et al* is presented for the $^2\Sigma^+$ states in figure 1. Similar behavior is observed for the $^2\Pi$ and $^2\Delta$ states.

A more informative method of considering the Rydberg states as a function of inter-nuclear distance R is to look at quantum defects directly. This method makes it easy to assess completeness in terms of the number of states found in the calculation and to identify so-called intruder states, which are valence states whose effective quantum number changes rapidly as function of R. These are presented in figure 2 for the $^2\Sigma^+$, $^2\Pi$, and $^2\Delta$ symmetries. For the $^2\Sigma^+$ state, the quantum defects show a stronger than usual (Rabadán and Tennyson 1997) dependence on R due to many intruder states, which result in avoided crossings among various BeH states. These appear as characteristic kinks in the PECs, which can be seen from figure 1. For other symmetries, the dependence of the quantum defects on R is much less pronounced.

3.2. Resonances as a function of bond length

In I we presented the resonance positions and widths at the BeH^+ equilibrium bond length $R_e = 2.5369\,a_0$. Here we give a fuller and more systematic calculation of the resonances as a function of the bond length. The resonance curves of total symmetry $^2\Sigma^+$, $^2\Pi$, and $^2\Delta$ are shown in figure 3. Resonances that cross the ion ground state become bound and these are shown in each figure as starred lines below the $X\ ^1\Sigma^+$ ground state of the BeH^+ ion.

The resonance curves in the R-matrix calculation correspond to neutral dissociative states in the diabatic picture. Such diabatic calculations have been performed by Roos *et al* (2009). The diabatic curves of Roos *et al* are also shown in figure 3 for comparison. We find similarity, though not complete agreement, between our curves and those of Roos *et al*. Since the models used for the two studies are different, direct comparisons are difficult. Roos *et al*'s MRCI calculations for the target curves used a smaller CAS and target basis than ours, meaning, for instance, that they were only able to characterize a single $^2\Delta$ resonance state that appears to be too low in energy relative to the BeH^+ ion ground state. For the scattering calculation they used the MRCI target curves and complex Kohn variational method to obtain the resonant states. Our resonance curves appear somewhat different from

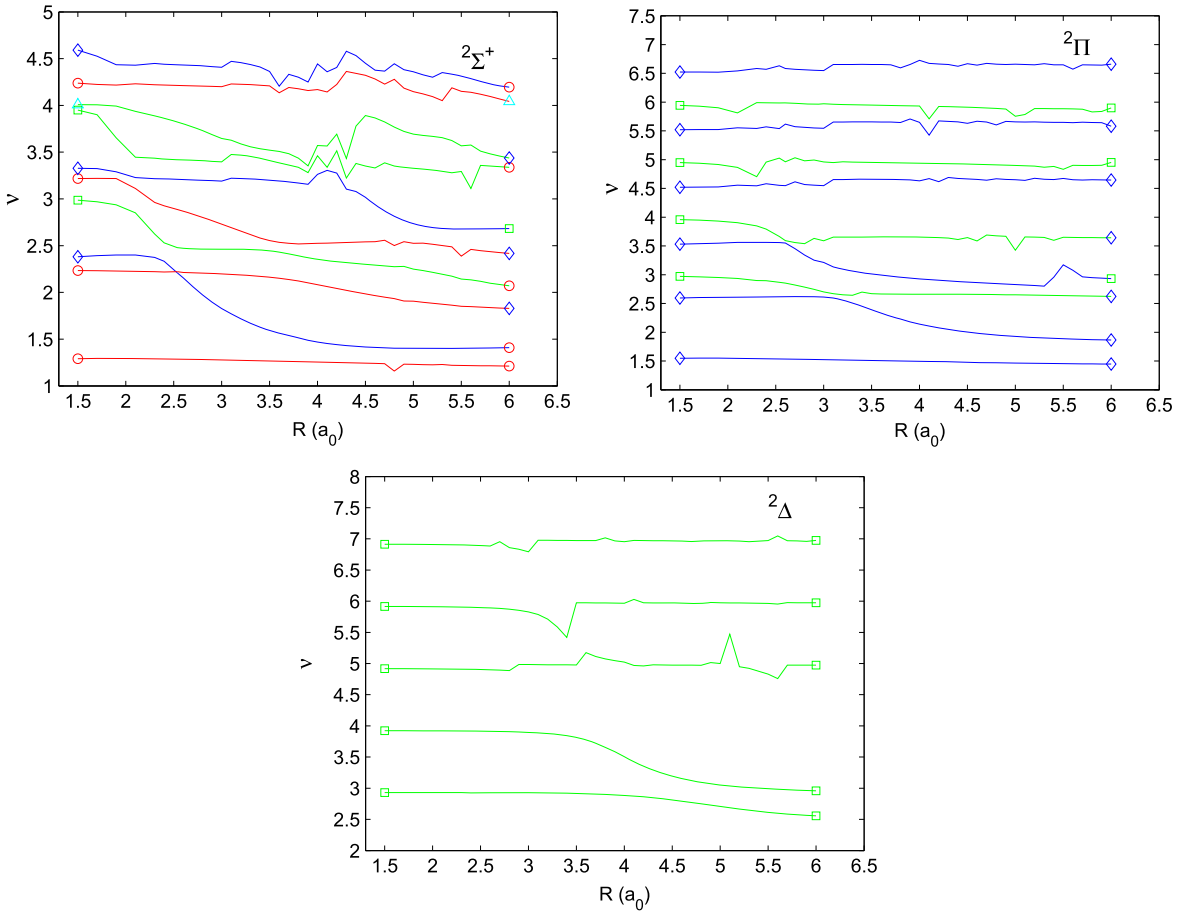

Figure 2. Effective quantum numbers for the BeH states of $^2\Sigma+$, $^2\Pi$, and $^2\Delta$ symmetry as a function of inter-nuclear distance R. The nature of the states is indicated with the symbols ∘: s-state, ◊: p-state, □: d-state, and Δ: f-state.

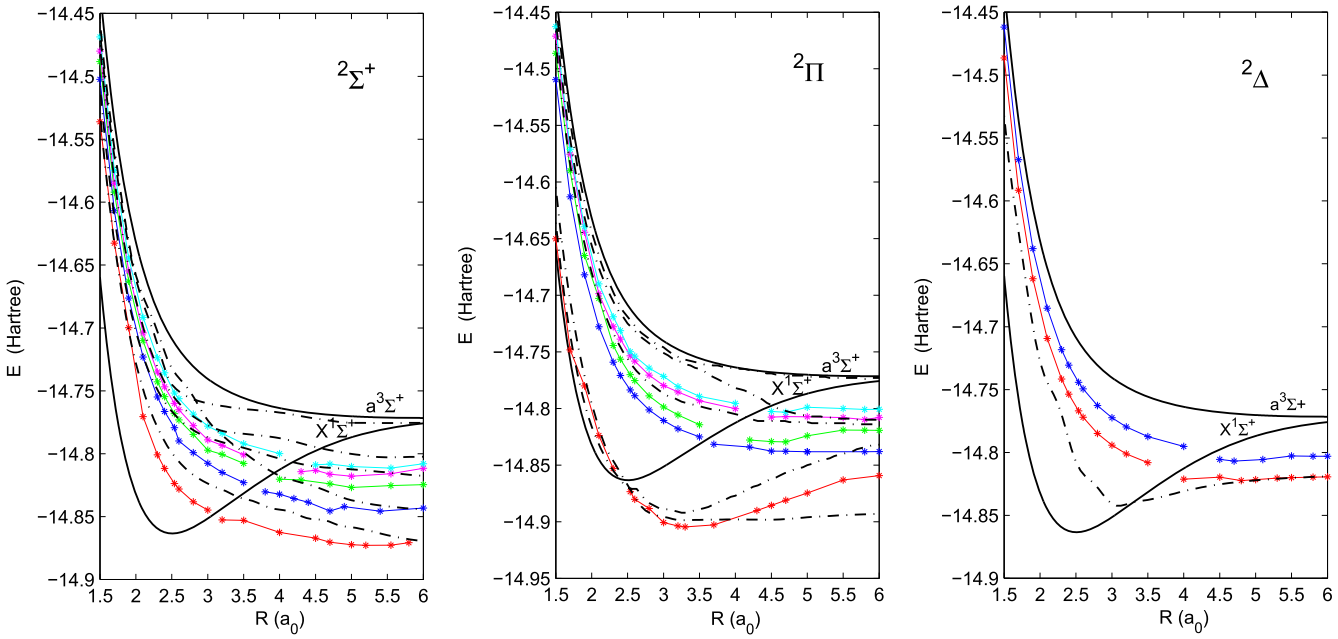

Figure 3. BeH resonances as a function of inter-nuclear distance R and total symmetry as indicated in each figure. The lowest black continuous curve is the $X\,^1\Sigma^+$ ground state of the BeH^+ ion. Resonances that cross the ion ground state become bound and these are shown as starred lines of the same color as that of the corresponding resonances. The quasidiabatic potentials of Roos *et al* (2009) (dash-dotted curves) are also shown.

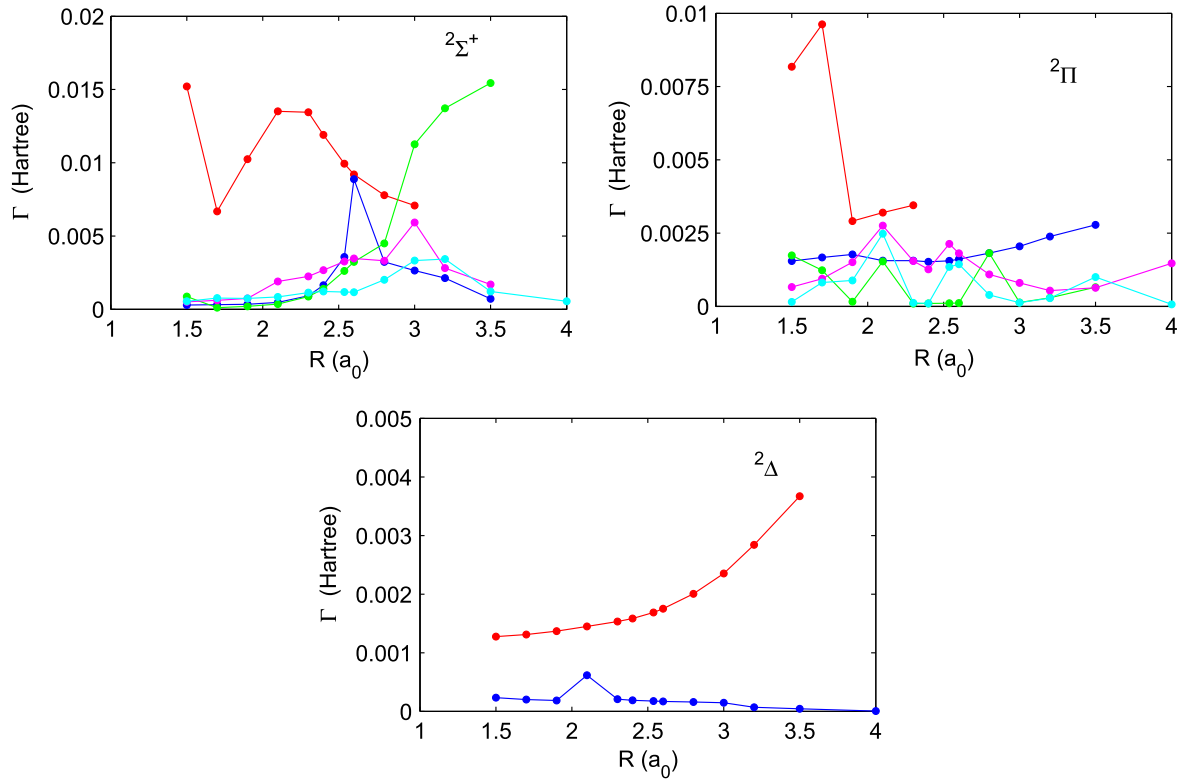

Figure 4. Resonance widths corresponding to the resonances shown in figure 3 as a function of internuclear distance R. The total symmetry of the resonant states is as indicated in the figure.

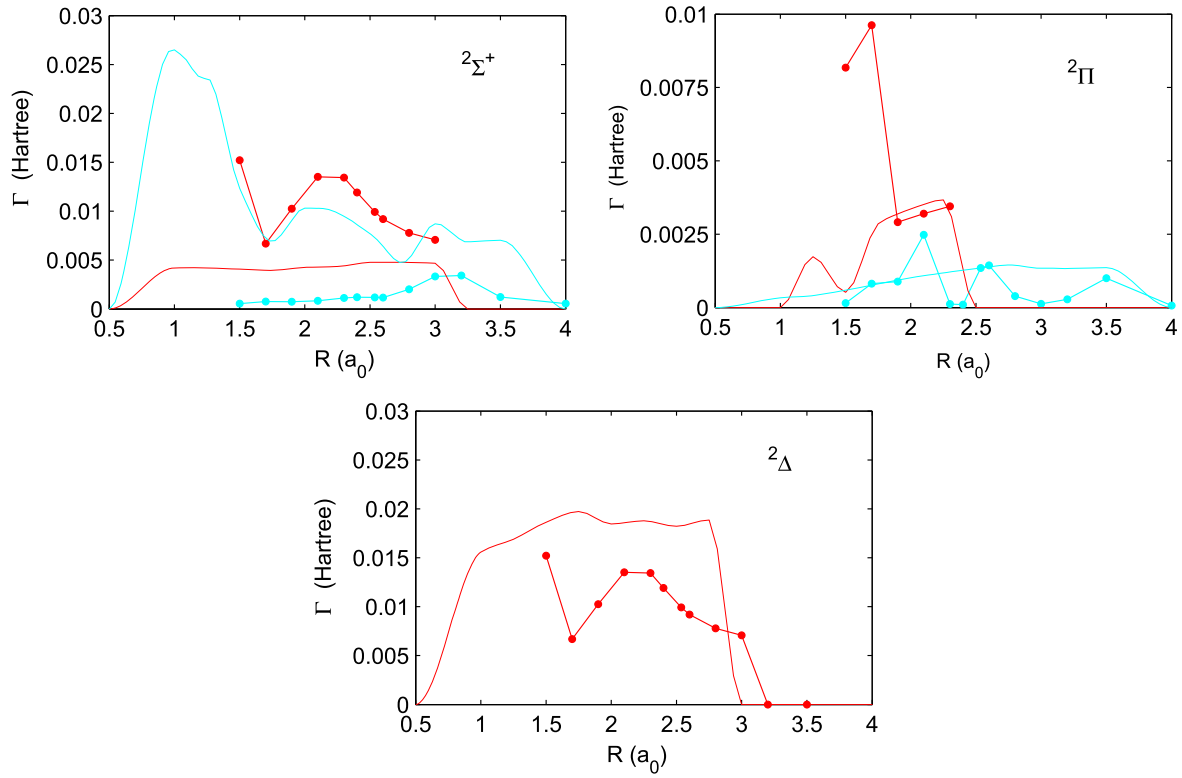

Figure 5. Comparison of resonance widths for the highest and lowest resonances of each symmetry indicated in the panels. Lines with symbols: present work. Thin lines without symbols: Roos *et al* (2009).

those of Roos *et al*, particularly with respect to the crossing point of the resonance curves with the BeH^+ ion ground state. For example, our lowest $^2\Sigma^+$ resonance curve crosses the ion at a lower energy than the corresponding $^2\Sigma^+$ resonance curve of Roos *et al* (see figure 3). Since DR is very sensitive to this crossing, the lower crossing point of this $^2\Sigma^+$ resonance curve may result in significant differences in the calculated DR cross-section compared to that obtained by Roos *et al*.

Figure 4 presents the resonance widths that correspond to the resonances given in figure 3. Since the widths are inversely proportional to their lifetimes, the resonance widths eventually become zero as the resonance crosses the ion and continues into a bound state. Roos *et al* (2009) present electronic couplings $V(R)$ for some of the states, which are related to the resonance widths $\Gamma(R)$ through the relation $V(R) = \sqrt{\Gamma(R)/2\pi}$. Figure 5 compares our resonance widths with those of Roos *et al* for the highest and lowest resonances of each symmetry. The widths are similar, although ours show more structure, which is a result of the avoided crossings (see Little and Tennyson 2013 for example). It would appear that Roos *et al* constrained their resonances to have zero width at small R. In general, resonances get broader at short bond lengths, and this feature is likely to affect computed DR cross-sections, particularly from excited vibrational ion states (see, e.g., the recent dissociative attachment study of Laporta *et al* 2015).

4. Conclusion

To summarize, we have calculated the potential energy curves for the $^2\Sigma^+$, $^2\Pi$, and $^2\Delta$ symmetries of the BeH molecule in the framework of the R-Matrix method. Our PECs compare well with earlier calculations of Petsalakis *et al* (1992, 1999). An important characteristic of electron collision with molecular ions is the appearance of a series of Feshbach resonances. We calculated the resonance positions and widths for the e-BeH^+ system as a function of geometry. Continuation of resonances as bound states below the ion was also traced. A comparison of our resonance curves with the recent calculations of the diabatic BeH dissociative curves of (Roos *et al* 2009) was also presented.

Ion curve and quantum defects of the Rydberg series converging to the ion, resonance curves, and their associated widths provide the starting point for DR calculations. These were all provided in the present work. Similar data were calculated previously by Roos *et al* (2009) and used to calculate DR cross-sections. However, we found some important differences between our resonance curves and widths and those of Roos *et al*. Recently, *ab initio* molecular data (Little and Tennyson 2013, 2014) obtained by the R-Matrix method have been successfully used to calculate DR of the N_2^+ ion by Little *et al* (2014). Hence, we expect that the present data can be used to produce better and more reliable DR cross-sections, which will be the subject of future work.

Acknowledgments

We thank Jose Sánchez-Marín for communicating the FCI data in electronic form. We also thank Ioan Schneider for many helpful discussions.

References

Bagus P S, Moser C M, Goethals P and Verhaegen G 1973 *J. Chem. Phys.* **58** 1886–97
Ballance C P, McLaughlin B M, Nagy O, Berrington K A and Burke P G 1998 *J. Phys. B: At. Mol. Opt. Phys.* **31** L305–14
Barnett A R 1982 *Computer Phys. Comms.* **27** 147–66
Burke P G 2011 *R-Matrix Theory of Atomic Collisions* (Berlin: Springer)
Buttle P J A 1967 *Phys. Rev.* **160** 719–29
Chakrabarti K and Tennyson J 2012 *Eur. Phys. J.* D **66** 31
Cooper D L 1984 *J. Chem. Phys.* **80** 1961
Henriet C and Verhaegen G 1984 *J. Mol. Struct.* **107** 63–73
Henriet C and Verhaegen G 1986 *Phys. Scripta.* **33** 299
Laporta V, Celiberto R and Tennyson J 2015 *Phys. Rev.* A **91** 012701
Little D A and Tennyson J 2013 *J. Phys. B: At. Mol. Opt. Phys.* **46** 145102
Little D A and Tennyson J 2014 *J. Phys. B: At. Mol. Opt. Phys.* **47** 105204
Little D A, Chakrabarti K, Mezei J Zs, Schneider I F and Tennyson J 2014 *Phys. Rev.* A **90** 052705
Machado F B C, Roberto-Neto O and Ornellas F R 1998 *Chem. Phys. Lett.* **284** 293–9
Merola M, Escourbiac F, Raffray R, Chappuis P, Hirai T and Martin A 2014 *Fusion Engg. Des.* **89** 890
Morgan L A 1984 *Comput. Phys. Commun.* **31** 419
Morgan L A, Tennyson J and Gillan C J 1998 *Computer Phys. Commun.* **114** 120–8
Noble C J and Nesbet R K 1984 *Computer Phys. Comms.* **33** 399–411
Petsalakis I D, Theodorakopoulos G and Nicolaides C A 1992 *J. Chem. Phys.* **97** 7623–8
Petsalakis I D, Papadopoulos D, Theodorakopoulos G and Buenker R J 1999 *J. Phys. B: At. Mol. Opt. Phys.* **32** 3225–37
Pitarch-Ruiz J, Sánchez-Marín J and Valesco A M 2007 *J. Comput. Chem.* **29** 523–32
Pitarch-Ruiz J, Sánchez-Marín J, Valesco A M and Martin I 2008 *J. Chem. Phys.* **129** 054310
Rabadán I and Tennyson J 1996 *J. Phys. B: At. Mol. Opt. Phys.* **29** 3747–61
Rabadán I and Tennyson J 1997 *J. Phys. B: At. Mol. Opt. Phys.* **30** 1975–88
Roos J B, Larsson M, Larson Å and Orel A E 2009 *Phys. Rev.* A **80** 012501
Sarpal B K, Branchett S E, Tennyson J and Morgan L A 1991 *J. Phys. B: At. Mol. Opt. Phys.* **24** 3685–99
Tennyson J 1988 *J. Phys. B: At. Mol. Opt. Phys.* **21** ‘805–816
Tennyson J 2010 *Phys. Rep.* **491** 29–76
Tennyson J and Morgan L A 1999 *Phil. Trans. Royal Soc. London* A **357** 1161–73
Tennyson J and Noble C J 1984 *Comput. Phys. Commun.* **33** 421–4
Zhang R, Baluja K L, Franz J and Tennyson J 2011 *J. Phys. B: At. Mol. Opt. Phys.* **44** 035203